Device Simulation for NANO MOSFET and Scaling issues

Young June Park, Seonghoon Jin , Sung-Min Hong and Hong Shick Min
School of Electrical Engineering and NSI_NCRC
Seoul National University, Seoul, Korea,

Abstract

For understanding of the device operations and its interaction with the circuit in the nano scale era, the device simulation has been extended to include the quantum transport effects, statistical effects and to be compatible with the circuit simulation environments. To do so, the full Newton scheme has been developed to fully integrate the Poisson equation, transport equation and the Schrodinger equation in the NANOCAD[1], which is the in-house developed program for the 2 and 3 dimensional device simulator. The method is applied to the nano scale Double Gate(DG) MOSFET structure showing that the quantum effect in the transport direction as well as in the vertical direction is important. Also, the CLESICO[2] system has been developed to treat the nodes in the device same as the nodes in the circuit, thereby the effects of the internal physics in the device on the circuits can be readily understood. The method is applied to understand the effects of the thermal noise of the MOSFET channel in the RF mixer and the local oscillator.

Introduction

As the MOSFET channel length is scaled down in the sub 40nm scheme, the quantum effects such as the quantum confinement effects in the vertical direction and the quantum tunneling effects lateral direction of the channel become more important. Also, the detailed physics in the device become more transparent to the circuit environments as the rail to rail voltage level is reduced while the noise level in the device is not scaled. The extension of the numerical device simulator to include the proper quantum transport effects and the coupled device/circuit simulation (mixed mode simulation) open the new horizon to the new paradigm of the device design and analysis for the MOSFET device and circuits in the nano scale regime.

For this, we have developed the NANOCAD software to find the a self-consistent solution of the Schr¨odinger, Poisson, and carrier transport equations[1]. Also, the CLESICO system, the mixed mode simulation environment to solve the semiconductor equations and the circuit equation(KCL and KVL) using the harmonic balance techniques[2].
In the NANOCAD environment, a fully coupled Newton scheme [3] is applied to solve the Schr¨odinger, Poisson, and carrier transport equations simultaneously. In this way, the numerical error and difficulty(or slow) in the numerical convergence in the decoupled method could be largely improved. In the next section, the application of the algorithm to 2DEG/DG(Density Gradient) mode analysis of the silicon based DG MOSFET will be presented, where the Schr¨odinger equation is solved in the confinement direction and the quantum corrected transport equation is solved in the transport direction.

In the CLESICO system, the devices are discretized as in the conventional device simulators. The semiconductor equations (i.e. Poisson equation and the electron and hole continuity equations) are solved in the frequency domain using the harmonics balance (HB) technique [4]. The iterative matrix solver, generalized minimum residual method (GMRES)[5], is exploited since the size of the system is too large to deal with the direct solver. We use the 'quasi-static Jacobian,' which neglects the time derivatives of the governing equations for the system including the semiconductor equations, as a prescaler. We find out that the method is very effective and numerically efficient in decoupling the components originated from different sampled components in the time domain up to a few hundreds GHz range. For the noise analysis in the CLESICO, the system is linearized to obtain the conversion Green's functions (CGFs) by an aid of the generalized adjoint approach [6]. As an example, we consider the RF mixer with the two-dimensional MOSFETs and will show that the simulations give the correlation between the detailed physics in the MOSFET's such as the noises and the circuit performances.

DG MOSFET simulation

As an example of the 2DEG/DG mode analysis of the DG MOSFET shown in fig.1, the two-dimensional Schr¨odinger equation is divided into the confinement (y-coordinate) and transport (x-coordinate) directions.
The electron density in each subband, $N_{ki,}$ is obtained by the quasi-Fermi energy (E_{kFi}) and the quantum potential.

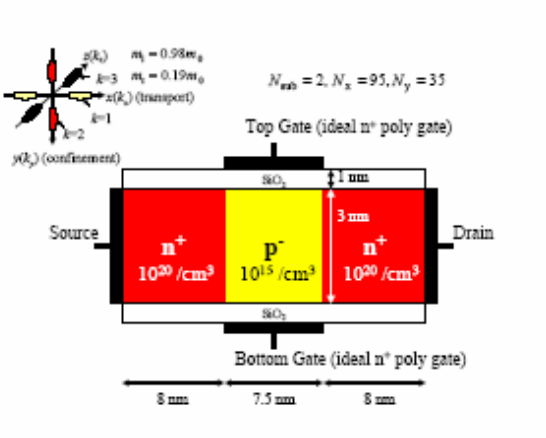

Fig. 1 Schematic of the thin body DGFET structure. The device and crystal coordinates are aligned. The same bias is applied to the top and bottom gates.

Fig. 2 shows the overall Jacobian matrix to stand for the system of equations in the coupled manner. The unknowns are the variables, V , ψ_k , ,E_{ki} , $\sqrt{N_i^k}$, and E^k_{Fi}, which are the electrostatic potential, the waver function, energy eigenvalue, area density, and Fermi level (of kth subband), respectively.

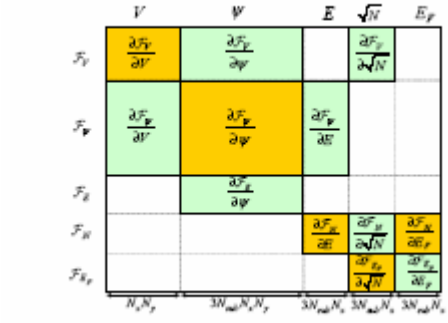

Fig. 2.Schematic of the Jacobian matrix. The total number of unknowns is $((1 + 3N_{sub})N_xN_y + 9N_{sub}N_x)$. Note that each block matrix is very sparse.

Fig. 3 and 4 show the area density of electrons and the energy level of the subbands along the channel. In the figures, the comparisons are made with the more comprehensive quantum transport model called the NEFG model[7,8]built in NANOCAD. It can be shown that the DG/DEG model accurately and efficiently simulate the internal physics as well as the IV characteristics(not shown in this paper).

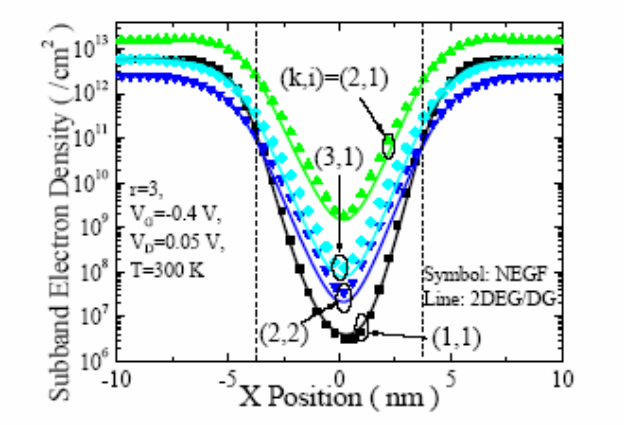

Fig. 3. Subband electron densities along the channel predicted by the 2DEG/DG (line) and NEGF (symbol) models.

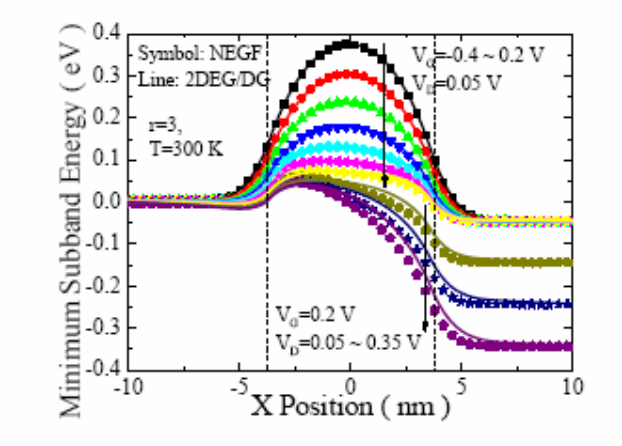

Fig. 4 Bias dependence of the minimum subband energy level predicted by the 2DEG/DG model (line) and the NEGF model (symbol). The gate bias is first increased from -0.4 V to 0.2 V with the drain bias fixed to 0.05 V, and then the drain bias is increased from 0.05 V to 0.35 V.

RF mixed mode simulation

As an example of the mixed mode simulation using the CLESICO system, the effects of the diffusion noise sources of the MOSFET channel to the RF mixer are simulated. The circuit considered in this work is the single-balanced RF CMOS mixer with 2 resistors and three MOSFETs as shown in Fig. 5. The output is taken as a differential voltage from drains of two LO transistors. The number of the unknowns per a sampling time is about 24,000. Since the number of the harmonics is set to 10, the whole system has about a half million unknowns. The magnitude and fundamental frequency of the LO signal is 0.15 V and 1 GHz, respectively. We found that the conversion gain from the 1.1 GHz RF signal to the output at 0.1GHz is 1.33.

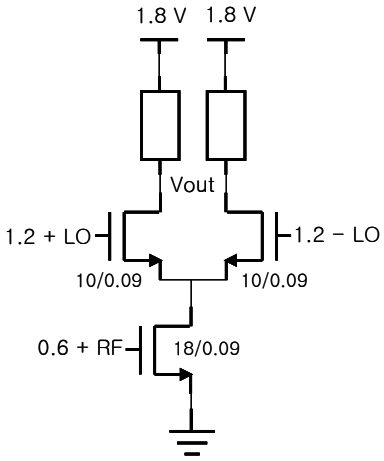

Fig. 5 Circuit schematic of the single-balanced down-conversion mixer.

The CGF(Conversion Green Function) for the mixer output noise voltage at 0.1 GHz corresponding to the (modulated) electron noise source is calculated. Fig. 6 shows the CGF for 1.1 GHz noise source in the RF port MOSFET. The noise source in the drain side has strong impact on the mixer output noise. Fig. 7 also shows the same quantity in the left LO port MOSFET. Contrary to Fig. 6, the noise source in the source side has a strong impact on the mixer output noise since the frequency down-conversion from 1.1 GHz to 0.1 GHz takes place in the channel in the LO port MOSFET. Similar studies have been performed to understand the CGFs for other frequency components of the noise such as 0.1 GHz noise source (no frequency conversion) in the RF port and LO port MOSFET. The effect of the noise source only in the drain side of the LO port MOSFET is found to be dominant because the frequency conversion is not needed in this case.

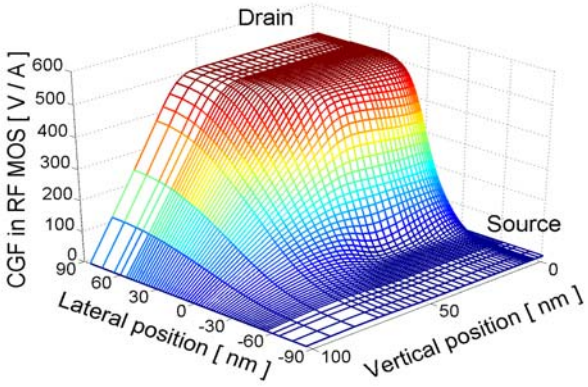

Fig. 6. CGF for 1.1 GHz noise source in the RF port MOSFET.

In Fig. 8 and 9, we plot the CGFs along the channel in the RF port MOSFET and LO MOSFET,respectively.

In this way, the detailed contribution of the noises originated from each device (and passive elements) to the output noise can be known. In this example, the power spectral density of the mixer output noise voltage is calculated to be 20.2 $(nV)^2/Hz$, among which 55 % comes from the RF port MOSFET and the other comes from the LO port MOSFETs (the noise from two resistors are not considered).

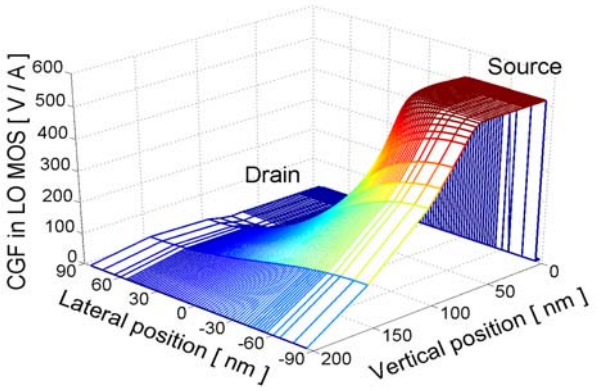

Fig. 7. CGF for 1.1 GHz noise source in the left LO port

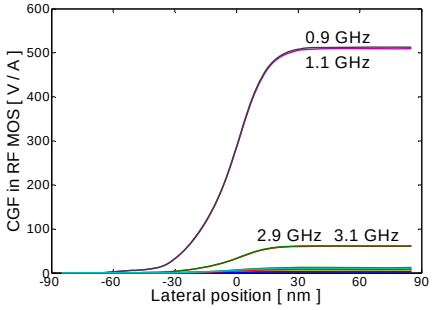

Fig. 8. CGFs along the channel in the RF port MOSFET.

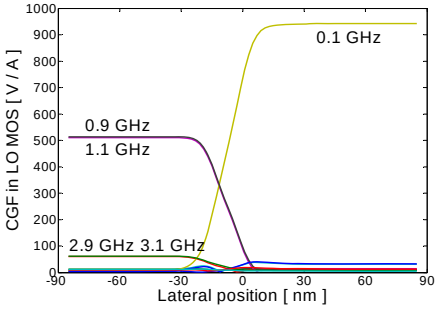

Fig. 9. CGFs along the channel in the left LO port MOSFET.

Conclusion

In this work, we have developed the coupled scheme for the Schrodinger equation , transport equations and the Poisson equation. The scheme is successfully applied to the modal approach for the DG MOSFET structures. Also, the physics based TCAD framework, CLESICO, is developed to perform the mixed mode simulation in the circuit environments. The method is applied to the mixer circuits used to down convert the RF signals. It is shown that the detailed internal physics in the devices and their interactions with the circuit node can be known .
It is believed that the approaches will render more profound tool for the analysis and design of the nano scale MOSFET devices and circuits.

Acknowledgement

This work was supported by the National Core Research Center program of the Korea Science and Engineering Foundation (KOSEF) through the NANO Systems Institute and Seoul National University.

References

[1] S. Jin, Y. J. Park, and H. S. Min, "A full Newton scheme for coupled Schrodinger, Poisson, and Design Gradient Equations,", in *Intl. Conference on Simulationof Semiconductor Processes and Devices*, Tokyo, Sept. 2005, p. 295.
[2] S. Hong, R.Kim, C.Park, Y. J. Park, and H. S. Min, "A Physics based TCAD framework for noise analysis of RF CMOS circuits under the large signal operations,"in *Intl. Conference on Simulationof Semiconductor Processes and Devices*, Tokyo, Sept. 2005, p. 119.
[3] J. M. Ortega and W. C. Rheinboldt, *Iterative solution of nonlinear equations in several variables*. San Diego, CA: Academic Press, 1970.
[4] B. Troyanovsky, Ph.D. Dissertation, Stanford University, 1997.
[5] Y. Saad *et al.*, "GMRES: a generalized minimal residual method for solving nonsymmetric linear systems," *SIAM Journal on Scientific and Statistical Computing*, vol. 7, pp. 856–869, 1986.
[6] F. Bonani, S. D. Guerrieri, G. Ghione and M. Pirola, *IEEE Trans. Electron Devices*, vol. 48, pp. 966-977, 2001.
[7] S. Datta, *Electronic Transport in Mesoscopic Systems*. Cambridge: Cambridge University Press, 1995.
[8] Z. Ren, "Nanoscale MOSFETs: Physics, simulation and design," Ph.D.
dissertation, Purdue Univ., West Lafayette, IN, USA, Dec. 2001.

NANO device simulation and modeling

Young June Park, Director
NSI_NCRC, Seoul National University

21st Century COE Program
Fourth Hiroshima International Workshop on
Nanoelectronics for Tera-Bit Information Processing
September 16 (Friday), 2005

Motivation(1)

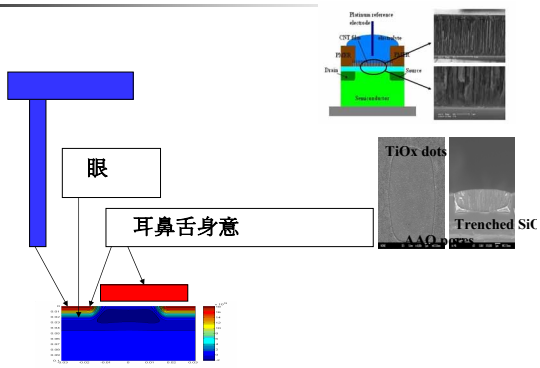

Motivation(2)

Carrier transport for IV
, speed: energy of carriers

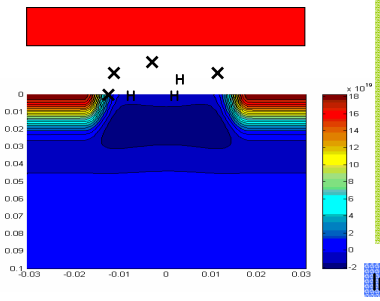

-How carrier generates free H
-How H interacts with SiO2 defects
-How the defects model explains

*SILC
*1/f noise
*and the leakage current
in statistical and consistent way

Interaction with circuits

Motivation(3)

•NANOCAD:
- For Quantum and Hydrodynamic Modeling(o)
- with Monte Carlo for statistical modeling (o)
- and short/long term reliability and noise modeling(ox)
- including the atomistic molecular physics in the gate(oxx)

•CLEISCO framework for circuit-device interaction
-RF modeling(o)
-Noise modeling(o)
-eventually merged with NANOCAD (x)

Structure of the DRAM cell transistor

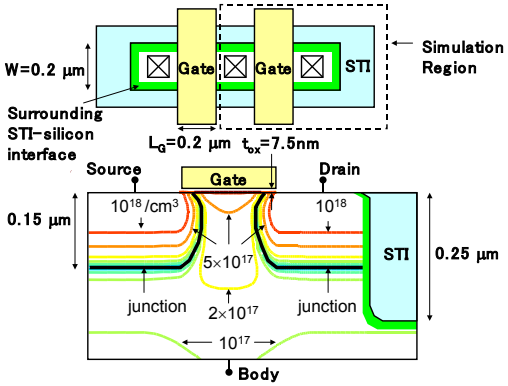

Green's function Method for the Leakage Current

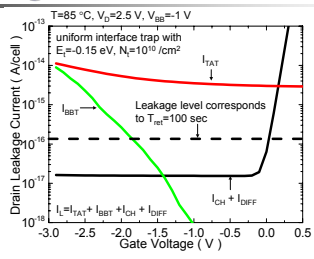

- The TAT current component can be calculated using Green's function as

$$I_{TAT} = -\sum_{j=1}^{N} R_{trap}\left(\mathbf{r}_j, E_j\right)\left\{G_n\left(\mathbf{r}_j\right) + G_p\left(\mathbf{r}_j\right)\right\}$$

- Other components can be obtained before the MC simulation.

Effects of Mechanical Stress

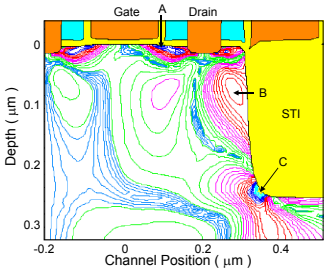

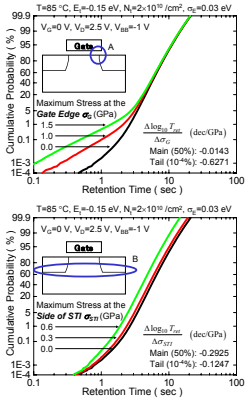

Monte Carlo (MC) modeling for Electron-Electron (EE) scattering

- EE scattering
  - a hot electron source of deep sub-micron device
  - MC is the most effective method for EE scattering simulation
- Multiplication
  - Split one MC electron into copied electrons
  - Weights are aligned to all the copied electrons
- Propose **Baby Electron Addition (BEA)** technique
  - Technique for weight redistribution after EE scattering
  - The conservation of energy, momentum and charge is guaranteed by additional of an electron after scattering

Baby Electron Addition (BEA) technique

$$w_1E_1 + w_2E_2 = w_2E'_1 + w_2E'_2 + (w_1 - w_2)E_1$$

(E : physical quanatity, w_i : Multiplication weight of i-th particle. Assume $w_1 > w_2$)

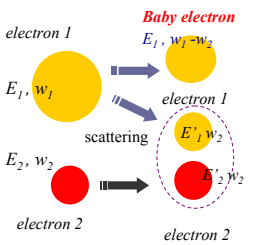

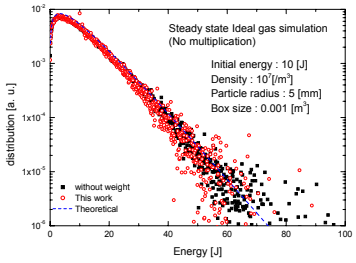

Verification : Energy distribution of random weight ideal gas. Collisions between weighted molecules are realized by BEA technique.

Application : TEHD model considering EE scattering

- Tail Electron Hydro Dynamics (TEHD) considering EE (uniform bulk)

$$\frac{\partial n}{\partial t} \approx \frac{n}{\tau_{12}} - \frac{n}{\tau_{21}} - \frac{n}{\tau_{ee}} \approx n\left(\frac{1}{\tau_{12}} - \frac{1}{\tau_{21}} - \frac{1}{\tau_{ee}}\right) \approx \frac{n}{\tau'}$$

Tail electron density

Phonon absorption relaxation time | Phonon emission relaxation time | **EE scattering relaxation time**

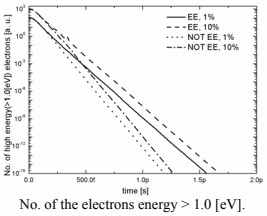

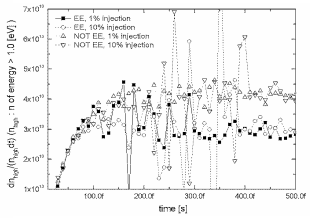

No. of the electrons energy > 1.0 [eV].
'EE' : considering EE scattering.
'NOTEE' : NOT considering e-e scattering.

$$\frac{1}{\tau_{ee}} \approx 10^{13}\,[s^{-1}], \quad \tau_{ee} \approx 0.1\,[ps]$$

Drain Bias Dependence of Drain Noise for Long Channel (Lmet=140nm)

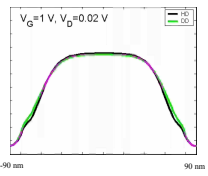

Effective Vector Green's Function

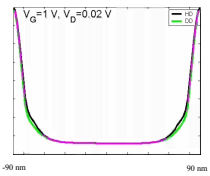

Local Noise Source

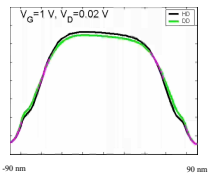

Areal Distribution of Noise Current

- As V_D increases further, the noise in the source section increases as the vector Green's function in the source section increases.
- The difference of vector Green's functions between HD and DD models confined in the drain section, where the noise source are negligible.

Drain Bias Dependence of Drain Noise for Short Channel (Lmet=40nm)

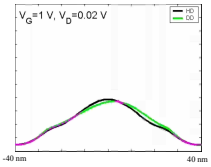

Effective Vector Green's Function

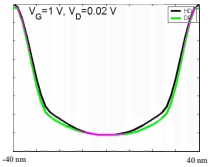

Local Noise Source

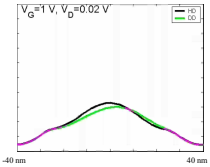

Areal Distribution of Noise Current

- Contrary to the long channel case, the vector Green's functions from HD and DD models become very different in the entire region if V_D increases.

Decomposition of Thermal Noise

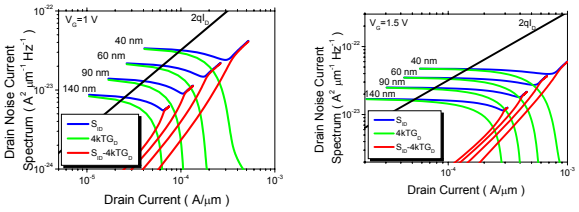

$S_{id} = 4kTG_D$ + excess noise term

As V_D increases, the excess noise term increases rapidly and it becomes dominant as V_D exceeds saturation voltage. Therefore, the behavior of S_{id} in the saturation region is due to the excess noise term.

Quantum Transport Models in NANOCAD

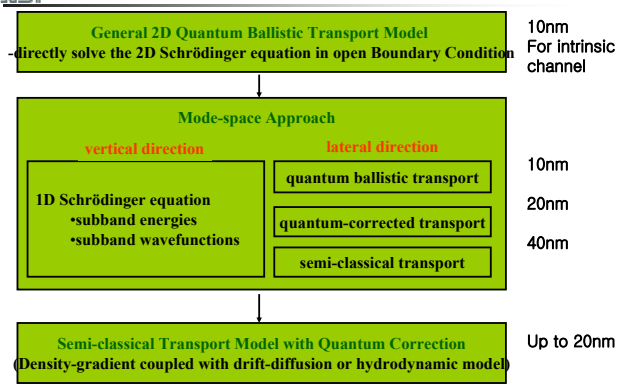

Introduction (1)

- Device Scaling of MOSFET V_G=1V, N_a=10^{18}/cm^3, t_{ox}=15Å
  - Channel Doping ↑
  - T_{ox} ↓
- Quantum Effect
  - Confinement
    - V_{th} ↑
    - C_{inv} ↓
  - Tunneling

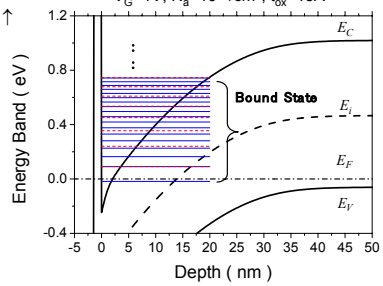

Introduction (2)

- Nonlocal Transport
  - E field variation ↑
  - Mean free path finite
- Energy Conservation
  - Energy gain in the device(due to field) = Energy loss to lattice + Energy loss to contact
  - DD model assumes that the energy gain is equal to the energy loss to lattice (not true in the scaled device).
- In the ballistic limit, mobility is not well defined (HD also fail)

Hydrodynamic density-gradient model

Derivation of HDG model

Wigner/Boltzmann Transport Equation

$$\frac{\partial f}{\partial t} + \mathbf{v}\cdot\nabla_r f - \sum_{l=0}^{\infty}\frac{(-1)^l(\nabla_r\cdot\nabla_k)^{2l+1}Vf}{\hbar 4^l(2l+1)!} = \left(\frac{\partial f}{\partial t}\right)_C$$

Multiplying 1, k, k^2 and integrating w.r.t. k ↓

Quantum Hydrodynamic Equations

relaxation time approx.
approx. of heat flux
near equilibrium approx. ↓

HDG Governing Equations

Effective Quantum Potential

- After derivation, we obtain a very similar equation set to HD model, except the effective quantum potential term

$$\psi_{\mathrm{qn}} = 2b_{\mathrm{n}} \frac{\nabla^2 \sqrt{n}}{\sqrt{n}}$$

- Driving force in the drift term

$$F_{eff} = -\nabla\left(\psi_{\mathrm{qn}} + \psi\right)$$

Governing Equations (1)

- Poisson Equation

$$-\nabla \cdot \left(\varepsilon \nabla \psi\right) - q\left(p - n + N_D^+ - N_A^-\right) = 0,$$

- Electron Continuity Equation

$$\nabla \cdot \mathbf{F} + U = 0$$

- Energy Balance Equation

$$\nabla \cdot \mathbf{S} - q\nabla\psi \cdot \mathbf{F} + U\frac{3}{2}k_B T + n\frac{3}{2}k_B \frac{T - T_0}{\tau_w} = 0,$$

- Quantum Potential Equation

$$\nabla \cdot \left(b\nabla\sqrt{n}\right) - \sqrt{n}\psi_{\mathrm{q}} / 2 = 0$$

Governing Equations (2)

- Electron Flux Density

$$\mathbf{F} = \mu n \nabla\left(\psi + \psi_q\right) - \mu\nabla\left(\frac{k_B T}{q} n\right),$$

- Electron Energy Flux Density

$$\mathbf{S} = -\kappa\nabla T + \frac{5}{2}k_B T\mathbf{F},$$

The Boundary Condition for the electrode

$\psi_{\mathrm{Si}} = \psi_0 + V_{\mathrm{bias}}$	Poisson's equation
$n = n_0$	Electron continuity equation
$\psi_{\mathrm{qn}} = 0$	Quantum potential equation
$T_{\mathrm{n}} = T_0$	Energy balance equation

Penetrating Boundary Condition for Si/SiO_2 Interfaces

▪ The electron density penetrated into oxide by x from the Si/SiO_2 interface can be approximated as

$$n(x) = n(0)\exp\left(-2x / x_p\right),$$

where n(0) is the electron density at the interface and

$$x_p = \frac{\mathrm{h}}{\sqrt{2m_{ox}\Phi_B}}$$

is the characteristic penetration depth calculated from WKB approximation.

Boundary Condition for Si/SiO_2 Interfaces

$\psi_{\mathrm{Si}} = \psi_{\mathrm{SiO_2}}$	Poisson's equation
$\mathbf{n} \cdot \mathbf{F} = 0$	Electron continuity equation
$\mathbf{n} \cdot b_{\mathrm{ox}} \nabla\sqrt{n} = -\left(b_{\mathrm{ox}} / x_{\mathrm{p}}\right)\sqrt{n_0}$	Quantum potential equation
$\mathbf{n} \cdot \mathbf{S} = 0$	Energy balance equation

1D MOSCAP Simulation

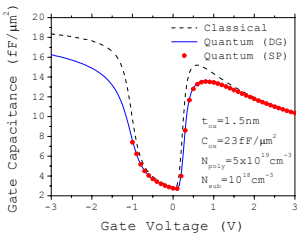

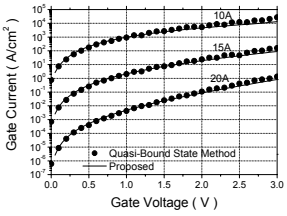

2D 25 nm NMOSFET Structure

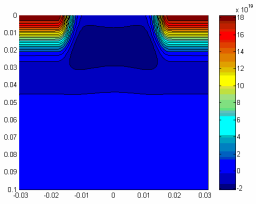

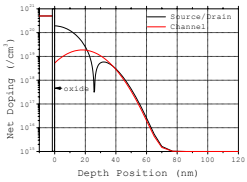

t_{ox}=1.5nm
L_{gate}=50nm
L_{eff}=25nm

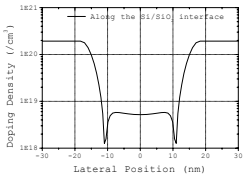

Quantum Potential and Electrostatic Potential

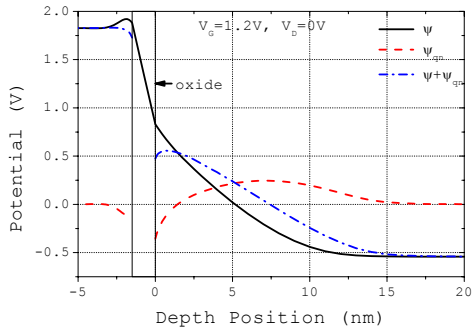

ID-VG Characteristics(effects of quantum In Hydro)

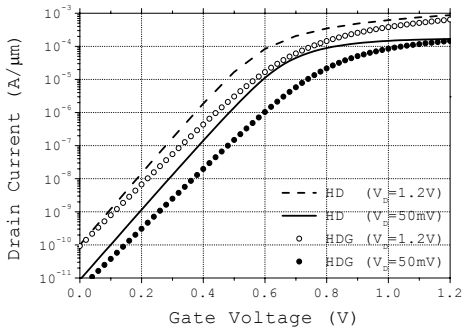

ID-VD Characteristics

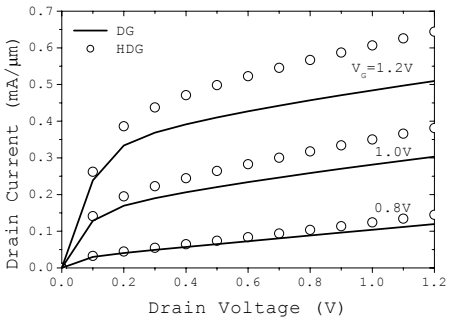

Electron average velocity in the channel

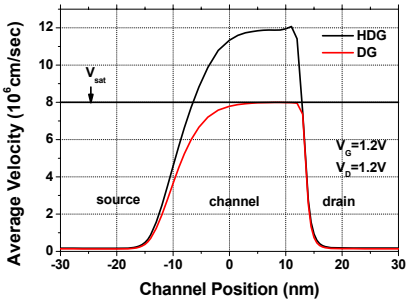

Quantum mechanical model

- Full Quantum and ballistic
- Mode Space approach with
  - * Drift diffusion
  - * Hydro dynamic

2D Quantum Ballistic Transport Model

- Directly solve the coupled **Poisson** and **Schrödinger** equation using the finite element method for arbitrary shaped device domain in **open B.C.**

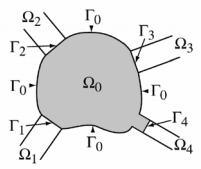

device region: Ω_0
lead: Ω_1 ,…, Ω_4
device boundary: Γ_0
device/lead boundary: Γ_1, …, Γ_4

$$-\nabla\cdot\left(\frac{\varepsilon}{q}\nabla V\right)+q\left(p-n+N\right)=0$$

iteration

$$-\frac{\hbar^2}{2}\left[\frac{\partial}{\partial x}\left(\frac{1}{m_x^*}\frac{\partial\Phi}{\partial x}\right)+\frac{\partial}{\partial y}\left(\frac{1}{m_y^*}\frac{\partial\Phi}{\partial y}\right)\right]+V(\mathbf{r})\Phi(\mathbf{r})=E\Phi(\mathbf{r})$$

2D Quantum Ballistic Transport Model

- Boundary condition at the leads

$$\Phi(\eta_i,\xi_i)=\sum_1^N\chi_m^i\left[a_m^ie^{-ik_m^i\eta_i}+b_m^ie^{ik_m^i\eta_i}\right]+\sum_{N+1}^{\infty}\chi_m^i\left[a_m^ie^{\kappa_m^i\eta_i}+b_m^ie^{-\kappa_m^i\eta_i}\right]$$

- **where χ_m is the solution of the coupled 1-D Poisson and Schrödinger equations at the lead *i***

$$\begin{cases}-\frac{d}{d\xi_i}\left[\varepsilon(\xi_i)\frac{dV(\xi_i)}{d\xi_i}\right]=\rho(\xi_i)\\ -\frac{\hbar^2}{2}\left[\frac{d}{d\xi_i}\left(\frac{1}{m_{zi}^*}\frac{\partial\chi_m^i(\xi_i)}{\partial\xi_i}\right)\right]+V(\xi_i)\chi_m^i(\xi_i)=E_m^i\chi_m^i(\xi_i)\end{cases}$$

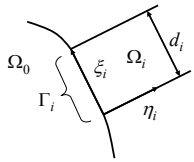

The local coordinate system in lead *i* region

2D Quantum Ballistic Transport Model

- **Sampling of the Density of State**: Calculate sine and cosine like bound states (standing wave solution) and eigenenergies (Laux et al.)
  ⇒ Decompose these eigenstates into the traveling states

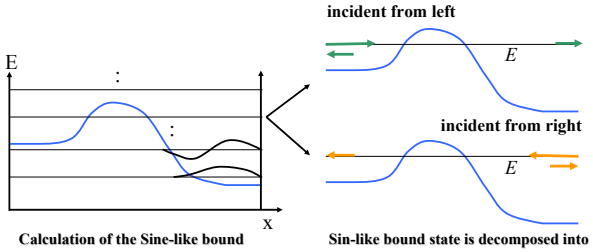

Calculation of the Sine-like bound states

Sin-like bound state is decomposed into traveling wavefunctions

Mode-space Approach

- The 2-D Schrödinger equation is divided into the confinement (y) and transport direction (x).

$$-\frac{\hbar^2}{2}\frac{\partial}{\partial y}\left(\frac{1}{m_y^k}\frac{\partial\psi_{ik}}{\partial y}\right)+\left(V(x,y)-E_{ik}(x)\right)\psi_{ik}=0$$

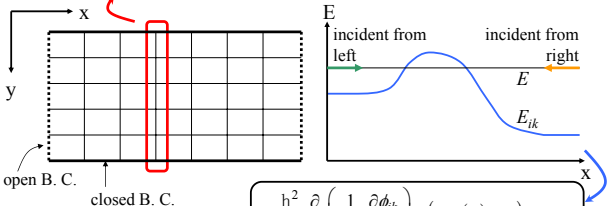

$$-\frac{\hbar^2}{2}\frac{\partial}{\partial x}\left(\frac{1}{m_x^k}\frac{\partial\phi_{ik}}{\partial x}\right)+\left(E_{ik}(x)-E\right)\phi_{ik}=0$$

Semi-classical Transport with Quantum Correction

- Effective quantum potential is derived from the Wigner distribution function ⇒ its gradient acts as a driving force

$$\psi_{qn}=2b_n\frac{\nabla^2\sqrt{n}}{\sqrt{n}}$$

$$F_n=\mu_n n\nabla\left(\psi+2b_n\frac{\nabla^2\sqrt{n}}{\sqrt{n}}\right)-\mu_n\nabla\left(\frac{k_BT_n}{q}n\right)$$

- It is an approximate approach, which gives reasonable results when the quantum confinement effects are dominant.

Simulation Example (Structure)

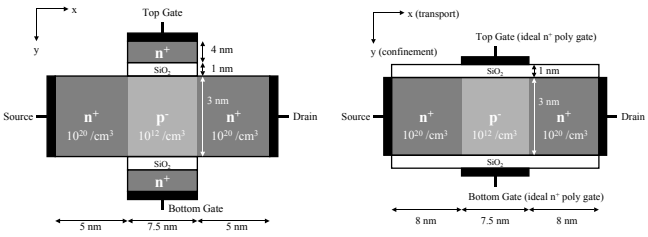

Schematic Structure of Non-ideal 7.5 nm Double-Gate MOSFET

Schematic Structure of ideal 7.5 nm Double-Gate MOSFET

2D Quantum Ballistic Transport Simulation Example

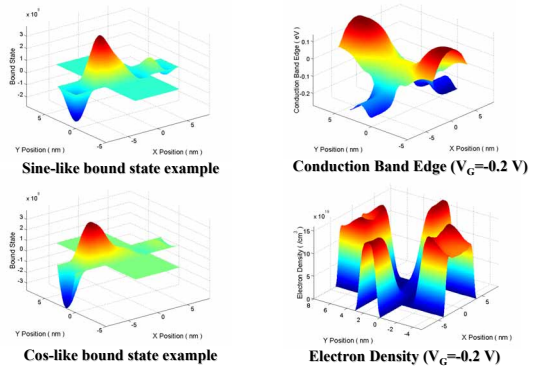

Sine-like bound state example

Conduction Band Edge (V_G=-0.2 V)

Cos-like bound state example

Electron Density (V_G=-0.2 V)

Mode-space Approach Example

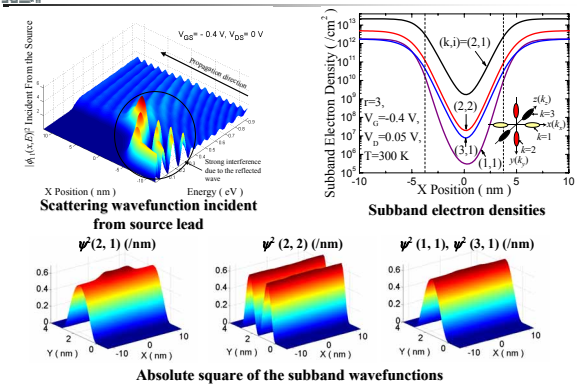

Scattering wavefunction incident from source lead

Subband electron densities

Absolute square of the subband wavefunctions

Quantum corrected Transport in Mode-space Approach Example

-1D Schrodinger equation and 1D density-gradient equation

$$N_{ki}(x) = \frac{g_k\sqrt{m_y m_z}\,k_B T}{\pi\hbar^2}\ln\left[1+\exp\left(\frac{E_{Fki}(x)-E_{ki}(x)-V_{Qki}(x)}{k_B T}\right)\right]$$

$$V_{Qki}(x) = -\frac{\hbar^2}{2m_x r}\frac{1}{\sqrt{N_{ki}(x)}}\frac{\partial^2\sqrt{N_{ki}(x)}}{\partial x^2}$$

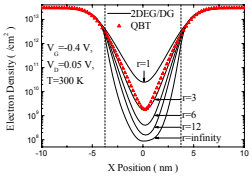

Comparison of the electron density

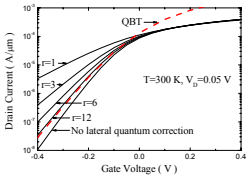

Comparison of the I_D-V_G characteristics

20nm and 10nm DG MOSFET

- The **scaling properties** of the DG-FET devices using the physics-based device simulation:
  following the **ITRS roadmap** from the 35 to 18 nm nodes for the high performance logic devices.
- Mode Space Approach:
  - the quantum confinement effects are considered by solving the **Schrödinger equation** in the confinement direction.
- In the transport direction:
  - **Drift-Diffusion Model**
    (μ_{low}=300 cm^2/V-sec, v_{sat}=1.035×10^{7}cm/sec)
  - **Hydrodynamic Model**
    (μ_{low}=300 cm^2/V-sec, v_{sat}=1.035×10^{7}cm/sec, τ_W=0.05 psec)
  - **Quantum Ballistic Transport Model**

DG-FET Structure

Scaling Parameters

- L_G(printed)
- L_G(physical)
- T_{ox}
- T_{si}
- V_{CC}

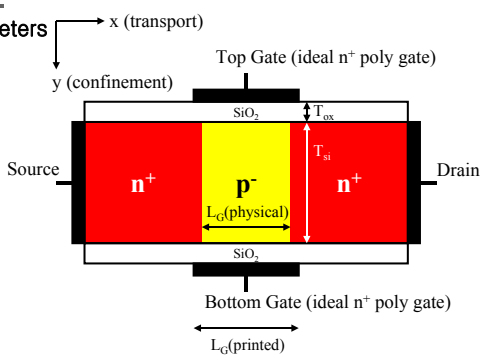

Scaling of DG-FET (ITRS Roadmap)

Year of production	2012	2013	2014	2015	2016	2017	2018
MPU ½ pitch (nm)	35	32	28	25	22	20	18
Printed gate length (nm)	20	18	16	14	13	11	10
Physical gate length (nm)	14	13	11	10	9	8	7
EOT (physical) (nm)	0.7	0.6	0.6	0.6	0.5	0.5	0.5
EOT(including poly dep.) (nm)	0.9	0.8	0.8	0.8	0.7	0.7	0.7
Power supply voltage (V)	0.9	0.9	0.9	0.8	0.8	0.7	0.7
Silicon thickness (nm)	10	9	8	7	6.5	5.5	5

- Silicon thickness is chosen to half of the printed gate length.
- Poly gate depletion effects are approximately taken into account by adding 0.2 nm to the EOT.

Quantum Confinement (Electron Density)

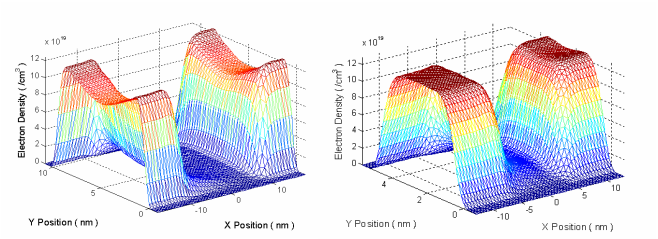

Electron density when T_{si}=10 nm (hp 35 node)

Electron density when T_{si}=5 nm (hp 18 node)

- Electron density near the interface decreases rapidly due to the quantum confinement effects.

Subband Energy Levels

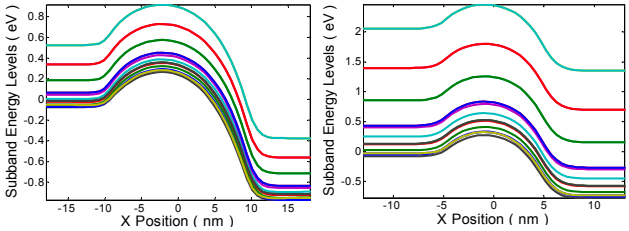

Subband Energy Levels (hp35 node, V_G=-0.5 V)

Subband Energy Levels (hp18 node, V_G=-0.5 V)

- 6 subbands per each valley (18 subbands in total) are considered in this work.
- Note that the spacing between the levels increases as the device is scaled down.

Subband Electron Densities

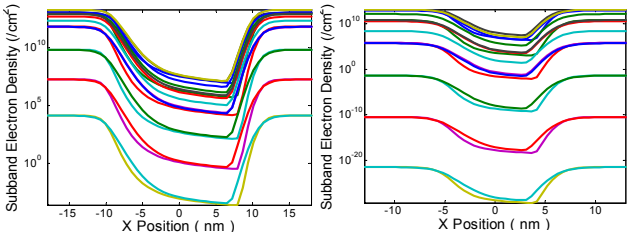

Subband Electron Density (hp35 node, V_G=-0.5 V)

Subband Electron Density (hp18 node, V_G=-0.5 V)

- The electron densities in the excited subbands decrease as the device are scaled down.

I_D-V_G Characteristics in Saturation

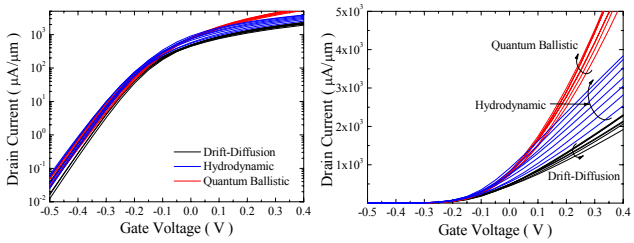

I_D-V_G Characteristics (log scale)

I_D-V_G Characteristics (linear scale)

I_D-V_G Characteristics in Saturation (continued)

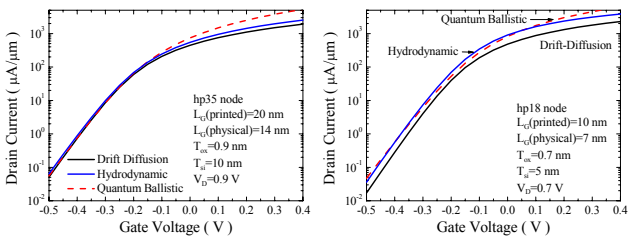

I_D-V_G Characteristics (hp 35 node)

I_D-V_G Characteristics (hp 18 node)

- It seems that the hydrodynamic model overestimate the drain current in the sub-threshold region (especially in the short-channel device)

Average Electron Velocity

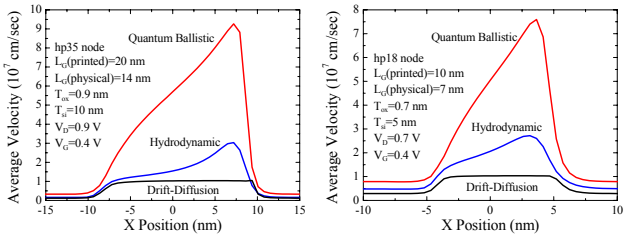

Average electron velocity (hp 35 node)

Average electron velocity (hp 18 node)

Threshold Voltage and the Saturation Current

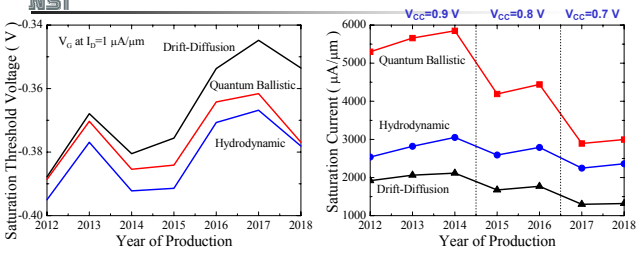

Predicted threshold voltage (V_G at I_D=1 μA/μm)

Predicted Saturation Current

- The difference in the threshold voltage between the drift-diffusion and quantum ballistic models increases as the scaling proceeds due to the source-to-drain tunneling effect.

CLEISCO

A Physics-Based TCAD Framework

for the Noise Analysis of RF CMOS Circuits

under the Large-Signal Operation

Device-circuit mixed-mode simulator with noise prediction capabilities

— supports the 2D (or 3D) numerical drift-diffusion device model and the lumped elements model.

— Both the shooting method or the harmonic balance (HB) method.

— calculate the periodic steady-state (PSS), the small-signal responses (PAC), and the noise performance (PNOISE) of the device-circuit mixed system.

— Both the quasi 2D model based on the SP method for >100 devices.

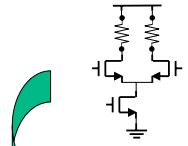

Circuit schematic

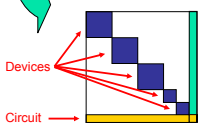

Nonzero pattern of Jacobian

Device-Circuit Coupling Scheme

A device-circuit coupling scheme [3] is used to handle the large system efficiently. Almost linear dependency of the linear system solution time on the number of the devices can be obtained without loss of accuracy in the Jacobian.

J_{dev}	0	J_V	$\delta\varphi$
$-G$	$I_{N,N}$	0	δI
0	0	$I_{N,N}$	δV

$$J_{dev}\delta\varphi + J_V\delta V = 0$$
$$\delta I = G\delta\varphi$$
$$\delta V = \delta V_{cir}$$

J_{dev}	0	J_V	$\delta\varphi$
0	$I_{N,N}$	$-G_{eq}$	δI
0	0	$I_{N,N}$	δV

$$J_{dev}\delta\varphi + J_V\delta V = 0$$
$$\delta I = G_{eq}\delta V$$
$$\delta V = \delta V_{cir}$$

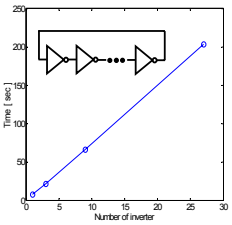

Linear system solution time versus the number of inverter

[2] K. Mayaram, and D. O. Pederson, IEEE TCAD, vol. 11, pp. 1003-1012, 1992.

Periodic Noise Analysis $G^i_{\delta v}(\vec{r};n,m)$

The conversion Green's function (CGF) [5]:

the effect of the noise source with frequency of $mf_L + f_s$ at position $\vec{r}$ in the i-th device on the output noise voltage with frequency of $nf_L + f_s$.

$$\delta v(nf_L + f_s) = \sum_{i=1}^{\#\ of\ devices} \sum_{m=-\infty}^{\infty} \int_V d\vec{r}\; G^i_{\delta v}(\vec{r};n,m)\; s(\vec{r};mf_L + f_s)$$

Noise source

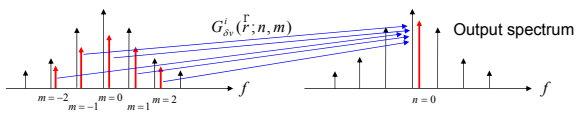

[5] F. Bonani, S. D. Guerrieri, G. Ghione, and M. Pirola, IEEE TED, vol. 48, pp. 966-977, 2001.

Example 1
- Noise in Single-Balanced Mixer

Single-Balanced Mixer: Down conversion mixer with 0.18um technology

- LO freq. 1 GHz, RF freq 1.1 GHz, IF freq. 0.1 GHz
- Amplitude of LO signal 0.3 V

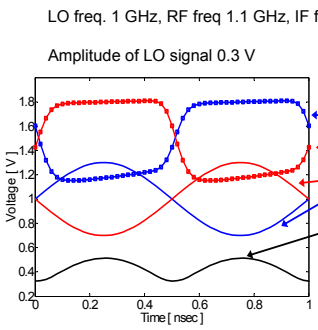

Output voltages of periodic steady-state solution without RF signal

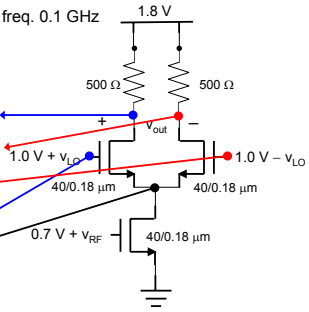

Circuit schematic of the single-balanced down-conversion mixer

Simulated Conversion Gain

The conversion gains for RF input is calculated by periodic small-signal analysis. The primary conversion gain from 1.1 GHz (RF freq.) to 0.1 GHz (IF freq.) is found to be 3.01 V/V.

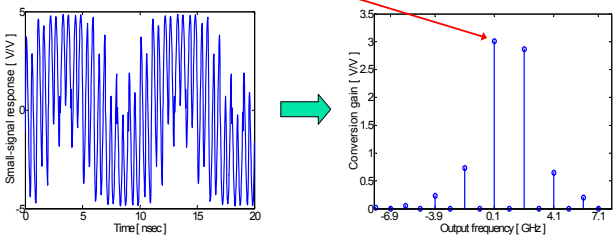

Small-signal response for 1.1 GHz RF input in time domain

Conversion gain for 1.1 GHz RF input in frequency domain

Conversion Green's Functions for RF Port MOSFET

In the RF port MOSFET, every noise component experiences the frequency conversion process before appearing in the output noise voltage.

- $G_{\delta V}^{RF}(\vec{r};0,1)$, CGF from 1.1 GHz (noise source) to 0.1 GHz (output voltage) in the RF port MOSFET is dominant.
- $G_{\delta V}^{RF}(\vec{r};0,0)$, CGF from 0.1 GHz (noise source) to 0.1 GHz (output voltage) in the RF port MOSFET is negligible (< 0.1 V/A).

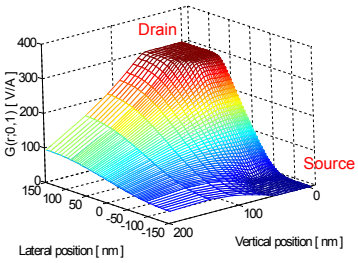

$G_{\delta V}^{RF}(\vec{r};0,1)$, CGF from 1.1 GHz to 0.1 GHz

Conversion Green's Functions for LO Port MOSFET

The frequency conversion process takes place in the channel of the LO port MOSFETs. In the LO port MOSFETs, only noise component near the source experiences the frequency conversion process before appearing in the output noise voltage.

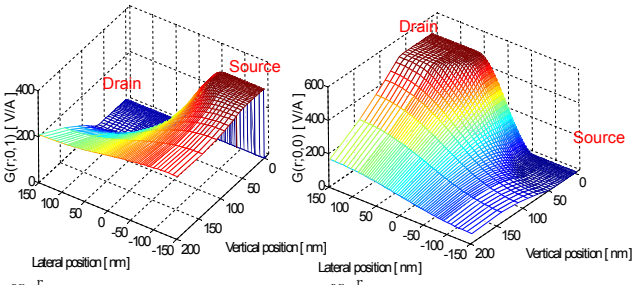

$G_{\delta V}^{RF}(\vec{r};0,1)$, CGF from 1.1 G to 0.1 G

$G_{\delta V}^{RF}(\vec{r};0,0)$, CGF from 0.1 G to 0.1 G

Spatial Contribution of Noise Source (HB results)

- The figures show the spatial noise contribution calculated from the HB code. Integrating over the device volume, we can obtain the total noise contribution of the device.
- The contribution from the RF port MOSFET to 0.1 GHz output noise voltage is found to be 20.2 $(nV)^2$/Hz.
- The contribution from two LO port MOSFETs to 0.1 GHz (IF) output noise voltage is found to be 16.5 $(nV)^2$/Hz.

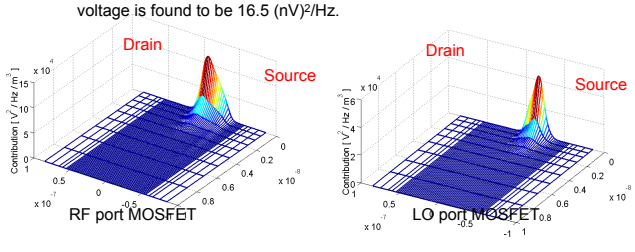

RF port MOSFET

LO port MOSFET

IV. Example 2
- Phase Noise in LC Oscillator

Conclusion

- **NANOCAD:**
  - Various models for quantum transport has been shown: space mode approach
    may be the best to connect from the DD to Quantum effects
  - Need a 'new mobility model' suitable to the 10nm.
  - A basis for the H generation from the carrier energy
  - Need to merge with MC to predict the statistical model
- **CLESICO**
  - Device/circuit simulation system has been proposed
  - Noise/reliability/nonlinearity from NANOCAD has to be implemented to CLESICO to understand the device/RF interaction

Periodic Small-Signal Analysis

Consider a circuit whose input is the sum of two periodic signals. Here one is an arbitrary periodic waveform with period T_L. The other is a "small" sinusoidal waveform with frequency f_s. Then,

$$v_s(t) = \sum_{n=-\infty}^{\infty} V_n^+ e^{j2\pi n f_L} e^{j2\pi f_s}$$

Then, the (complex) small-signal response v_s satisfies the following relation between two time points t and $t+T_L$.

$$v_s(t+T_L) = v_s(t)\exp(j2\pi f_s T_L) = v_s(t)\alpha^{-1}$$

This relation is employed for the boundary condition for the periodic small-signal analysis [4].

$$\begin{bmatrix} I & 0 & 0 & -\alpha I \\ -C_1/h & G_2+C_2/h & 0 & 0 \\ 0 & -C_2/h & G_3+C_3/h & 0 \\ 0 & 0 & -C_3/h & G_4+C_4/h \end{bmatrix} \begin{bmatrix} v_s(t_1) \\ v_s(t_2) \\ v_s(t_3) \\ v_s(t_4) \end{bmatrix} = \begin{bmatrix} 0 \\ u(t_2) \\ u(t_3) \\ u(t_4) \end{bmatrix}$$

[4] R. Telichevesky, K. Kundert, and J. White, DAC 1996, pp. 292-297, 1996.

Periodic Steady-State Analysis

The "matrix-free" shooting method [3] with GMRES is adopted.

$$\begin{bmatrix} I & 0 & 0 & -I \\ -C_1^k/h & G_2^k+C_2^k/h & 0 & 0 \\ 0 & -C_2^k/h & G_3^k+C_3^k/h & 0 \\ 0 & 0 & -C_3^k/h & G_4^k+C_4^k/h \end{bmatrix} \begin{bmatrix} -\delta x_1^k \\ -\delta x_2^k \\ -\delta x_3^k \\ -\delta x_4^k \end{bmatrix} = \begin{bmatrix} x_1^k - x_4^k \\ 0 \\ 0 \\ 0 \end{bmatrix}$$

Transient simulation

$$\Rightarrow \begin{cases} \left(I-\phi^k(4;1)\right)\left(-\delta x_1^k\right) = x_1^k - x_4^k \\ \phi^k(4;1) = \left(G_4^k+\dfrac{C_4^k}{h}\right)\times\dfrac{C_3^k}{h}\times\left(G_3^k+\dfrac{C_3^k}{h}\right)\times\dfrac{C_2^k}{h}\times\left(G_2^k+\dfrac{C_2^k}{h}\right)\times\dfrac{C_1^k}{h} \end{cases}$$

The state-transition matrix $\phi^k(4;1)$ are not calculated explicitly, therefore, we can avoid the operation with the dense matrix $\phi^k(4;1)$.

[3] R. Telichevesky, K. S. Kundert, and J. K. White, DAC 1995, pp. 480-484, 1995.

Oscillator Phase Noise Analysis

The perturbation projection vector (PPV) method [6] is adopted. The perturbation projection vector v_1 represents the effects of the noise sources on the oscillator phase deviation θ.

$$\frac{d\theta}{dt} = v_1^T(t+\theta(t))B(x_s(t+\theta(t)))b(t)$$

The timing jitter in one clock cycle has a variance cT.

$$cT = \int_0^T v_1^T(\tau)B(x_s(\tau))B^T(x_s(\tau))v_1(\tau)d\tau$$

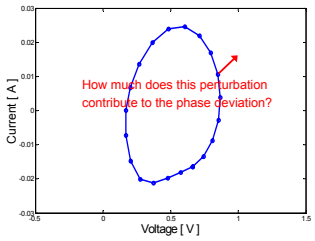

Limit cycle of an oscillator

[6] A. Demir, and J. Roychowdhury, IEEE TCAD, vol. 22, pp. 188-197, 2003.